



Tang, T-Y. D., Che Hak, C. R., Thompson, A. J., Kuimova, M. K., Williams, D. S., Perriman, A. W., & Mann, S. (2014). Fatty acid membrane assembly on coacervate microdroplets as a step towards a hybrid protocell model. *Nature Chemistry*, 6(6), 527-533. 10.1038/NCHEM.1921

Peer reviewed version

Link to published version (if available):
[10.1038/NCHEM.1921](https://doi.org/10.1038/NCHEM.1921)

[Link to publication record in Explore Bristol Research](#)
PDF-document

University of Bristol - Explore Bristol Research

General rights

This document is made available in accordance with publisher policies. Please cite only the published version using the reference above. Full terms of use are available:
<http://www.bristol.ac.uk/pure/about/ebr-terms.html>

Take down policy

Explore Bristol Research is a digital archive and the intention is that deposited content should not be removed. However, if you believe that this version of the work breaches copyright law please contact open-access@bristol.ac.uk and include the following information in your message:

- Your contact details
- Bibliographic details for the item, including a URL
- An outline of the nature of the complaint

On receipt of your message the Open Access Team will immediately investigate your claim, make an initial judgement of the validity of the claim and, where appropriate, withdraw the item in question from public view.

Fatty acid membrane assembly on coacervate micro-droplets as a step towards a hybrid protocell model

T-Y. Dora Tang,¹ C. Rohaida Che Hak,¹ Alexander J. Thompson,² Marina K. Kuimova,² D. S. Williams,¹ Adam W. Perriman¹ and Stephen Mann^{1*}

¹ Centre for Organized Matter Chemistry, School of Chemistry, University of Bristol, Bristol, BS8 1TS, UK. ² Chemistry Department, Imperial College London, Exhibition Road, London SW7 2AZ, UK.

*email: s.mann@bristol.ac.uk

Mechanisms of prebiotic compartmentalization are central to providing insights into how protocellular systems emerged on the early Earth. Protocell models are predominantly based on membrane self-assembly of fatty acid vesicles, although membrane-free scenarios involving liquid-liquid microphase separation (coacervation) have also been considered. Here we integrate these alternative models of prebiotic compartmentalization and develop a hybrid protocell model based on the spontaneous self-assembly of a continuous fatty acid membrane at the surface of preformed coacervate micro-droplets prepared from cationic peptides/polyelectrolytes and ATP or oligo-/polyribonucleotides. We show that the coacervate-supported membrane is multilamellar, and mediates the selective uptake or exclusion of small and large molecules. The coacervate interior can be disassembled without loss of membrane integrity, and fusion and growth of the hybrid protocells induced under conditions of high ionic strength. Our results highlight how notions of membrane-mediated compartmentalization, chemical enrichment and internalized structuration can be integrated in protocell models *via* simple chemical and physical processes.

The elucidation of plausible mechanisms of prebiotic compartmentalization offers important insights into how primitive processes of replication, metabolism and evolution could be materially embodied by spontaneous physical processes on the early Earth¹⁻³. Amongst several scenarios, the self-assembly of fatty acid vesicles has emerged as a dominant paradigm in the origin of life^{4,5}, and corresponding protocell models⁶ have established that archetypal properties, such as small-molecule diffusion⁷, macromolecular encapsulation and retention⁸, spatially confined catalysis and replication^{9,10}, membrane-mediated pH gradients¹¹, and competitive growth and division^{12,13}, can be associated with these simple self-assembled systems. Although these observations provide strong support for the protocell vesicle hypothesis, the model fails to account for the high encapsulation efficiencies required to produce appropriate representations of the molecularly crowded, chemically enriched, structured milieu that is a hallmark of cellular organization¹⁴. In contrast, Oparin suggested over fifty years ago that the spontaneous phase separation and chemical enrichment in water of counter-charged polyelectrolytes into liquid micro-droplets

(coacervates) could provide a mechanism of prebiotic compartmentalization that is facile and independent of membrane (vesicle) formation¹⁵.

Although numerous examples of biomolecular coacervation are known in synthetic systems¹⁶⁻¹⁸, protocell models based on liquid micro-droplet assembly have not advanced significantly since Oparin's initial experiments. However, a recent report demonstrated that coacervate micro-droplets with a range of biomimetic functions could be spontaneously assembled from aqueous mixtures of low molecular weight biologically relevant peptides and mononucleotides¹⁹. The peptide/nucleotide micro-compartments are stable between pH values of 2-10 and up to temperatures of 85°C, undergo pH-induced cycles of growth and decay, and comprise molecularly crowded aqueous interiors that are enriched in biomolecular components and display enhanced catalytic transformations. Significantly, the dielectric constant associated with the interior of the peptide/nucleotide droplets is lower than the surrounding continuous water phase, and as a consequence the micro-compartments exhibit selective molecular sequestration even though they are membrane-free^{19,20}.

The above studies, along with recent reports on liquid-liquid phase separation in living cells^{21,22}, biomolecular partitioning and gene expression in cell lysate coacervates²³, RNA catalysis in molecularly crowded aqueous two-phase polymer systems²⁴, and multi-enzyme iterative processing in polymer/nucleotide coacervate micro-droplets²⁵, suggest that it is timely to reconsider coacervate-mediated spatial compartmentalization and chemical enrichment as an alternative model of protocell organization. However, although the simplicity of coacervate assembly is attractive, the absence of an enclosing membrane is a major drawback of the model compared with vesicle-based approaches to micro-compartmentalization.

To address this concern, here we develop a hybrid protocell model based on the spontaneous self-assembly of a fatty acid membrane at the surface of preformed coacervate micro-droplets. We test the generality of our approach using binary combinations of short- or long-chain cationic peptides (oligolysine, polylysine) or a synthetic polyelectrolyte (polydiallyldimethylammonium chloride, PDDA) with a negatively charged monoribonucleotide (ATP) or mixture of oligo- and polyribonucleotides (RNA). We show that addition of sodium oleate at concentrations below the critical vesicle concentration results in the formation of membrane-bounded coacervate micro-droplets that we propose as the basis for a new type of protocell model. In particular, the membrane-delineated micro-compartments exhibit marked changes compared with uncoated coacervate droplets in their ability to sequester or exclude various solutes from the external medium, such that concentration gradients can be established across the surface of the hybrid protocells. The coacervate-supported membrane is multilamellar, has a viscosity comparable to free-floating oleate/oleic acid vesicles, and assembles specifically on the droplet surface under conditions not conducive to vesicle formation. We also demonstrate that the coacervate interior can be disassembled without loss of membrane integrity, and that fusion and growth of the hybrid protocells is induced under conditions of high ionic strength. Taken

together, our results indicate that fatty acid self-assembly and peptide/nucleotide coacervate formation can be assimilated into a novel protocell model that integrates notions of membrane-mediated compartmentalization, chemical enrichment and internalized structuration *via* the combination of simple chemical and physical processes.

Results and Discussion

Hybrid protocell construction and molecular uptake/exclusion properties. Positively charged coacervate micro-droplets were prepared at room temperature and neutral pH by direct mixing of aqueous solutions of oligolysine ($M_w = 0.5\text{-}2$ kDa), polylysine ($M_w = 15\text{-}30$ kDa) or PDDA ($M_w = 150$ kDa) in combination with a mixture of oligo- and polyribonucleotides (Torula yeast RNA, $M_w = 3\text{-}80$ kDa) or monomeric ATP under non-stoichiometric conditions (*see SI Methods*). Coacervates were routinely produced at the following approximate monomer molar ratios (charge ratios): polylysine : RNA (1 : 0.5), oligolysine : RNA (1 : 0.25), oligolysine : ATP (1 : 0.17) and PDDA : ATP (1 : 0.25). In each case, stable dispersions of liquid micro-droplets with diameters of a few to several tens of micrometres were observed by optical microscopy. Zeta potential measurements on the different types of coacervate droplets gave values in the range of +4 to +30 mV (Supplementary Fig. S1). Assembly of a fatty acid membrane on the surface of preformed polylysine/RNA, oligolysine/RNA or oligolysine/ATP micro-droplets was undertaken at pH 8.5-9.3 by the single-step addition of aqueous sodium oleate at concentrations below the critical micelle concentration (≈ 3 mM). A similar method was also used to prepare oleate-coated PDDA/ATP micro-compartments, although a two-step protocol was generally preferred at pH values above or equal to 10. In all cases, addition of oleate monomers resulted in charge reversal to produce fatty acid-coated micro-droplets with negative surface potentials (Supplementary Fig. S1).

Fluorescence microscopy was used to confirm the presence of a fatty acid membrane on the surface of each of the different types of coacervate micro-droplets (*see SI Methods*). For this, we employed a lipid soluble boron-dipyrin dye tagged with a 16-carbon chain (BODIPY FL C₁₆, Supplementary Fig.S2) as a fluorescent probe for bilayer formation²⁶⁻²⁸. In the absence of oleate, the dye was readily sequestered into the coacervate phase to produce micro-droplets that exhibited green fluorescence throughout their interior (Fig. 1a). As the solubility of the dye in water was very low, we attributed the preferential uptake to the reduced dielectric constant (ϵ) of the coacervate micro-droplet interior ($\epsilon \approx 55$) compared with the surrounding aqueous phase ($\epsilon \approx 80$)¹⁹. In contrast, BODIPY FL C₁₆-stained images of oleate-containing coacervate droplets at monomer molar ratios of 0.67 : 1 : 0.5, (oleate : polylysine : RNA), 0.67 : 1 : 0.25 (oleate : oligolysine : RNA), 0.8 : 1 : 0.17 (oleate : oligolysine : ATP) and 0.8 : 1 : 0.25 (oleate : PDDA : ATP) indicated that the dye was located specifically on the surface of the micro-compartments (Fig. 1b). To confirm the presence of an encapsulated coacervate phase, we prepared oleate/PDDA/ATP micro-droplets at a molar ratio of 1.6 : 1 : 0.25 that were doped with a blue fluorescently tagged ATP derivative (2',3'-O-(2,4,6-trinitrophenyl)adenosine-5'-triphosphate, TNP-ATP). Fluorescence optical

microscopy images showed blue fluorescence throughout the oleate-coated droplets (Figs 1c,d).

Dynamic light scattering (DLS) experiments performed on oleate-coated PDDA/ATP micro-droplets prepared at pH 10 showed a major peak at a mean hydrodynamic diameter (D_H) of 2 μm (Fig. 2a). A peak at $D_H = 2 \mu\text{m}$ was also observed for the uncoated micro-droplets (Fig. 2a), indicating no significant change in the diameter of the micro-droplets upon addition of oleate. This suggests that a continuous, ultrathin fatty acid shell, rather than for example an ensemble of discrete fatty acid vesicles surrounds the PDDA/ATP droplets. Significantly, as expected at pH 10, there was no evidence for a significant population of oleate micelles or vesicles in the coacervate dispersion (Fig. 2a). Similar observations were made for oleate-coated polylysine/RNA, oligolysine/RNA and oligolysine/ATP micro-droplets (Supplementary Figs S3 and S4).

Synchrotron radiation small angle X-ray scattering (SAXS) was used to obtain structural information on the membrane associated with the oleate/PDDA/ATP coacervate droplets prepared over a range of oleate concentrations at pH 10. Previous SAXS studies on the uncoated PDDA/ATP coacervate phase showed no evidence for long-range mesostructural order²⁹. In contrast, SAXS profiles from dispersions of the oleate/PDDA/ATP microdroplets at oleate concentrations at and above a monomer molar ratio of 0.6 : 1 : 0.25 showed two Bragg reflection peaks, including a sharp reflection at 5.46 nm and a broad reflection at 4.77 nm (Fig. 2b). The latter reflection could be deconvoluted into two or three peaks with closely related d spacings depending on the oleate/PDDA/ATP molar ratio (Supplementary Fig. S5). Similarly, SAXS investigations of oleate/oligolysine/ATP micro-droplets prepared at a molar ratio of 0.8 : 1 : 0.25 also showed two Bragg diffraction peaks with a minor reflection at 5.42 and a major peak at 4.90 nm (Supplementary Fig S6). Significantly, the SAXS profiles of the oleate/PDDA/ATP samples under excess water conditions showed a considerable increase in the intensity of the Bragg peak at 4.77 nm with increasing oleate concentration, whilst the reflection at 5.46 nm decreased slightly (Fig, 2b,c). SAXS profiles of oleate/PDDA/ATP micro-droplets (1.6 : 1 : 0.25, pH 10), which had been concentrated by approximately 30% by volume, indicated that the oleate membrane was multi-lamellar in structure (Fig. 2d). Six sharp, intense Bragg reflections were observed for the oleate-coated coacervate micro-droplets, and were assigned to two multi-lamellar phases with peak position ratios of 1 : 2 : 3, corresponding to Miller indices of (100), (200), (300) and repeat interlayer spacings, d , of 5.51 and 5.06 nm (Fig. 2d). SAXS profiles on control samples of oleic acid/oleate vesicles prepared at pH 8.5 showed a multi-lamellar structure with an interlayer spacing of *ca.* 5.5 nm (Fig. 2e). (See caption of Supplementary Fig 5 for a detailed analysis of the SAXS data).

The above observations were consistent with the self-assembly of oleate multilayers on the surface of the preformed coacervate micro-droplets. As a consequence, we expected the membrane-bounded micro-compartments to exhibit marked changes compared with uncoated micro-droplets in their propensity to uptake or exclude various solutes present in the external medium (*see SI Methods*). We tested this by using confocal fluorescence

microscopy to assess changes in the uptake of cationic, zwitterionic and anionic dyes, as well as cofactors such as β -nicotinamide adenine dinucleotide (NADH) (for molecular structures, see Supplementary Fig. S2), all of which readily partitioned into the interior of uncoated positively charged coacervate micro-droplets (Fig. 3). In contrast, anionic dyes such as calcein or fluorescein were excluded from the droplet interior in the presence of the negatively charged oleate membrane, such that confocal microscopy images of single droplets showed negligible fluorescence (Fig. 3). Uptake of the NADH dianion was also reduced, although some sequestration appeared to take place, suggesting that the fatty acid membrane restricted diffusion of the cofactor into the centre of the droplet. Positively charged dyes such as rhodamine 6G and the zwitterionic molecule Kiton red were also excluded from the droplet interior and bound specifically at the membrane surface, whilst uptake of the lower molecular weight cationic dye methylene blue was similar to that observed in the membrane-free micro-compartments (Fig. 3). Taken together, the results were consistent with the presence of a semi-permeable, negatively charged barrier at the surface of the oleate-coated coacervate micro-droplets, and indicated that concentration gradients could be established across the assembled fatty acid membrane.

Coacervate-mediated fatty acid membrane assembly. Studies on the mechanism of fatty acid membrane assembly on the surface of the polyelectrolyte/ribonucleotide micro-compartments were undertaken using positively charged PDDA/ATP micro-droplets prepared by a two-step procedure at a PDDA monomer : ATP molar ratio of 1 : 0.25. In the first stage, an aqueous solution of sodium oleate micelles prepared at pH 11 was added to an aqueous dispersion of positively charged PDDA/ATP coacervate droplets (pH 10.5) to give a final pH of 10, oleate final concentration of 1.5 mM, and oleate : PDDA : ATP monomer molar ratio of 0.32 : 1 : 0.25. Under these conditions, the total fatty acid concentration was below the critical micelle concentration (CMC, 3.0 mM at pH 10, equivalent to a molar ratio of 0.7 : 1 : 0.25), such that anionic oleate monomers interacted with the positively charged polyelectrolyte/ribonucleotide droplets. In the second stage, a single aliquot of the sodium oleate micelles was added to the oleate/PDDA/ATP droplet dispersion to give monomer molar ratios ranging from 0.4 : 1 : 0.25 to 2.4 : 1 : 0.25 at pH 10. Zeta potential measurements showed a progressive reduction in the positive surface charge of the droplets as the oleate concentration was increased in the coacervate dispersions (Fig. 4a). The droplets had an initial surface potential of +12 mV at a monomer molar ratio of 0 : 1 : 0.25, and became charge neutral at 0.6 : 1 : 0.25, which was below the CMC of the lipid. Higher levels of added oleate resulted in negative zeta potentials that became constant at a value of -60 mV at a molar ratio of 1.3 : 1 : 0.25. This value was similar to the potential recorded for oleate micelles alone at pH 11 (-65 mV). These observations were consistent with electrostatic binding of oleate monomers at the surface of the PDDA/ATP micro-droplets, followed by assembly of multiple fatty acid bilayers on the surface of the coacervate micro-compartments at higher lipid concentrations.

We used fluorescence microscopy to image the PDDA/ATP micro-droplets produced at various molar ratios of added oleate (Fig. 4b-e and Supplementary Fig. S7). Significantly, a homogeneous distribution of green fluorescence was observed throughout the droplets when BODIPY FL C₁₆ was added to micro-compartments treated with sub-CMC levels of oleate (oleate : PDDA : ATP monomer molar ratio = 0.32 : 1 : 0.25) (Fig. 4b). The images were analogous to those observed in the absence of oleate (see Fig. 1a), and indicated that the dye was able to access the droplet interior. Thus, binding of the oleate monomers to the positively charged droplets did not produce a continuous outer membrane bilayer under these conditions. In contrast, charge-neutral or negatively charged oleate/PDDA/ATP droplets prepared between molar ratios of 0.4 : 1 : 0.25 and 1.6 : 1 : 0.25 showed a heterogeneous distribution of dye with increased fluorescence intensity specifically on the surface of the micro-compartments (Fig. 4c-e), consistent with the formation of a fatty acid membrane. We attribute the formation of the membrane at pH values non-conducive to vesicle formation primarily to electrostatic interactions between the polyelectrolyte and oleate anions at the droplet surface that reduce intermolecular repulsions between the negatively charged fatty acid headgroups, which in turn lowers the monolayer interfacial curvature (See Supplementary Fig. S8 and S9 for further mechanistic details).

Given these observations, fluorescence lifetime imaging microscopy (FLIM) was used to determine the changes in local viscosities (η) associated with the assembly of the fatty acid membrane as well as the encapsulated PDDA/ATP coacervate matrix under different $x : 1 : 0.25$ molar ratios (*see SI Methods*). The PDDA/ATP matrix was probed using a coacervate-soluble molecular rotor (Kiton red)³⁰, which was sequestered into the positively charged micro-droplets prior to the addition of oleate. Alternatively, oleate-coated droplets were prepared without Kiton red and the lipid layer stained with BODIPY C₁₀, which served as a suitable molecular rotor for determining the viscosity of the fatty acid membrane³⁰⁻³². Significantly, the viscosity derived from the fluorescence lifetime of BODIPY C₁₀ in the oleate surface layer of the droplets decreased progressively as the amount of added oleate was increased until it reached a value of 20-40 cP (1 cP = 1 mPa.s), which was similar to that determined for a control sample of oleate/oleic acid vesicles ($\eta = 20-40$ cP) (Fig. 4f,g). In contrast, the local viscosity of the PDDA/ATP matrix associated with the fatty acid-coated micro-droplets was much lower (1-4 cP), and was not significantly influenced by the amount of added oleate (Fig. 4h). The values were similar to those determined for the coacervate matrix of uncoated droplets (2.8 ± 0.4 cP; $\eta(\text{H}_2\text{O}) \approx 1$ cP), indicating that encapsulation of the micro-droplets by the lipid membrane did not significantly influence the local structure of the phase-separated compartment. In comparison, values for the membrane and coacervate viscosities determined at the onset of membrane assembly and close to charge neutrality (0.6 : 1 : 0.25) displayed anomalously high lifetimes for BODIPY C₁₀ (1680 ps = *ca.* 140 cP), and two distinct viscosity domains for Kiton red (a short lifetime (< 1 cP) at the droplet centre) and a longer lifetime (> 4.5cP) at the edge of the micro-compartment (Fig. 4h). We attributed this to perturbations associated with the interaction of oleate with the coacervate matrix under charge neutral conditions (Supplementary Figure S10).

Hybrid protocell disassembly and growth. Internalized disassembly of the fatty acid-coated polyelectrolyte/ribonucleotide droplets with retention of the oleate membrane was achieved by dispersing the hybrid protocells in high ionic strength aqueous solutions (typically 75 mM). This was evidenced by FLIM experiments undertaken on oleate-coated PDDA/ATP micro-droplets prepared at pH 10 at an oleate : PDDA : ATP monomer molar ratio of 1.6 : 1 : 0.25 and stained with either BODIPY C₁₀, or Kiton red to measure the local viscosity of the fatty acid membrane and polyelectrolyte/ribonucleotide interior, respectively, under varying salt concentrations ([NaCl] = 0 to 100 mM) that alone produced no changes in the fluorescence lifetime (control experiments). The results showed that increasing the salt concentration gave a decrease in the fluorescence lifetime of Kiton red (Fig. 5a,b), which corresponded to a decrease in the viscosity of the encapsulated polyelectrolyte/ribonucleotide matrix from 2.7 ± 2.0 cP (no salt) to < 1 cP, consistent with progressive disassembly of the PDDA/ATP coacervate phase. This was consistent with control experiments undertaken on uncoated droplets dispersed in high ionic solutions (Supplementary Fig. S11). In contrast, the local viscosity of the fatty acid membrane associated with the oleate-coated droplets increased in the presence of higher salt concentrations, suggesting that the bilayer structure was more compacted due to charge screening between the oleate headgroups (Fig. 5c). Control experiments on oleic acid/oleate vesicles were in agreement with these observations (Supplementary Fig. S11).

The above results indicated that disassembly of the coacervate droplet core could be accomplished at salt concentrations of 75 mM without loss of the oleate multilayer membrane to produce fatty acid vesicles containing a concentrated aqueous solution of encapsulated polyelectrolyte and ribonucleotide molecules. However, fluorescence microscopy images of BODIPY FL C₁₆-stained, fatty acid-coated PDDA/ATP micro-droplets (1.6 : 1 : 0.25) incubated with higher concentrations of salt (100 mM NaCl) at pH 10 indicated that under these conditions the micro-compartments aggregated and fused to produce densely packed multilamellar “onion” vesicles^{33,34} (Fig. 5e,f) along with release of ATP to the external medium (Supplementary Fig. S12).

Conclusions

Using simple physical and chemical processes, we have demonstrated a new type of hybrid protocell model based on the spontaneous self-assembly of a continuous fatty acid multilamellar membrane at the surface of preformed coacervate micro-droplets comprising molecularly crowded interiors. The approach integrates notions of membrane-mediated compartmentalization, chemical enrichment and internalized structuration, and brings together alternative models of prebiotic compartmentalization based on either phase-separated liquid droplets^{15,19} or fatty acid vesicle self-assembly^{4,5,9,10}. Our studies indicate that the membrane-enclosed coacervate micro-compartments are semi-permeable and exhibit uptake and exclusion properties different from the uncoated micro-droplets. Thus, it should be possible to exploit the hybrid protocell model to develop trans-membrane control

of coacervate-sequestered reaction systems such as gene-directed protein synthesis²³ or RNA catalysis²⁴ by diffusion-limited regulation of the uptake of small molecules from the external continuous aqueous phase.

Our studies include membrane-bounded coacervate droplets that are constructed from low molecular weight components such as cationic oligopeptides, ATP and oligoribonucleotides. Such molecules along with fatty acids can be considered as prebiotically relevant, suggesting that our hybrid protocell model is a plausible hypothesis for origin of life research that needs to be further considered and developed. For example, although fatty acid membrane assembly depends on the initial presence of preformed positively charged coacervate micro-droplets under the experimental conditions investigated, it seems feasible that less stringent conditions might apply in the presence of highly heterogeneous mixtures of single chain amphiphiles, monoribonucleotides and low molecular weight oligo-RNAs. Indeed, compositional diversity is expected to be a hallmark of prebiotic environments, such that complex combinations of fatty acids with different chain lengths and headgroup chemistries, mononucleotides and nucleotide-derived cofactors (FAD, NADH etc) with different nucleobase moieties and charge densities, and polyelectrolytes with variable polarity and solubility, could provide a diverse landscape of mechanisms for the spontaneous formation of membrane-delineated coacervate-based protocellular constructs. Although the development of combinatorial methods for exploring the design, construction, function and evolutionary potential of model protocells is in its infancy, such an approach should offer important insights into the mechanisms of prebiotic compartmentalization on the early Earth.

Acknowledgements. We thank the Engineering and Physical Sciences Research Council (EPSRC, UK) and European Research Council (Advanced Grant) for financial support. We thank the EPSRC for a Career Acceleration Fellowship (grant number: EP/E038980/1) to MKK and the Malaysian government for the award of a PhD studentship to CRC. We acknowledge the Wolfson Bioimaging Facility (Mr. A. Leard) for assistance with confocal microscopy, beamline I22 (Dr. Nick Terrill and Mr. Andrew Smith) at Diamond Light Source, Dr. W. Briscoe for beamtime, and Prof. R. Richardson and Dr. M. Thomas for assistance and use of software for X-ray analysis. We thank Dr. W. Briscoe and Prof. J. Eastoe for helpful discussions.

Author contributions: SM, AWP, T-YDT, MKK, DSW conceived the experiments; CRCH, AJT, T-YDT performed the experiments; T-YDT, AJT, CRCH undertook the data analysis; T-YDT, AJT, CRCH, SM wrote the manuscript.

CRCH and AJT contributed equally to the work.

Competing financial interests

The authors declare no competing financial interests.

References

1. Rasmussen, S. Chen, L.H. Nilsson, M. & Abe, S. Bridging nonliving and living matter. *Artif. Life*. **9**, 269–316 (2003).
2. Luisi, P. The emergence of life, (Cambridge University Press, 2006).
3. Mann, S. Systems of creation: the emergence of life from nonliving matter. *Acc. Chem. Res.* **45**, 2131-2141 (2012) .
4. Deamer, D.W. & Barchfeld, G.L. Encapsulation of macromolecules by lipid vesicles under simulated prebiotic conditions. *J. Molecul. Evo.* **18**, 203–206 (1982)
5. Monnard, P.A. & Deamer, D.W., Membrane self-assembly processes: steps toward the first cellular life. *Anat. Record.* **268**, 196–207 (2002)
6. Dzieciol, A.J. & Mann, S. Designs for life: protocell models in the laboratory. *Chem. Soc. Rev.* **41**, 79-85 (2012).
7. Deamer, D.W. & Dworkin, J.P. Chemistry and physics of primitive membranes. *Top. Curr. Chem.* **259**, 1–27 (2005).
8. Apel, C.L., Deamer, D.W. & Mautner, M.N., Self-assembled vesicles of monocarboxylic acids and alcohols: conditions for stability and for the encapsulation of biopolymers. *Biochim. Biophys. Acta.* **1559**,1–9 (2002).
9. Oberholzer, T., Wick, R., Luisi, P.L. & Biebricher, C.K. Enzymatic RNA replication in self-reproducing vesicles: an approach to a minimal cell. *Biochem. Biophys. Res. Commun.* **207**, 250–257 (1995).
10. Mansy, S.S., Schrum, J.P., Krishnamurthy, M., Tobe, S., Treco, D.A. & Szostack, J.W. Template-directed synthesis of a genetic polymer in a model protocell. *Nature* **454**, 122-125 (2008).
11. Chen, I.A. & Szostak, J.W. Membrane growth can generate a transmembrane pH gradient in fatty acid vesicles. *Proc. Natl. Acad. Sci. USA.* **101**, 7965–7970 (2004).
12. Zhu, T.F., Adamala, K., Zhang, N. & Szostak JW. Photochemically driven redox chemistry induces protocell membrane pearling and division. *Proc. Natl. Acad. Sci. USA.* **109**, 9828–9832(2012).
13. Adamala, K. & Szostak, J.W., Competition between model protocells driven by an encapsulated catalyst. *Nature Chem.* **5**, 495-501 (2013).
14. Fulton, A.B., How crowded is the cytoplasm? *Cell* **30**, 345–347 (1982).
15. Oparin, A.I. (1953) *The Origin of Life* 2nd Ed, p 270 (Dover Publications, New York, 1953).
16. Evreinova, T.N., Karnaukhov, W.N., Mamontova, T.W., Ivanizki, G.R., The interaction of biological molecules in coacervate systems. *Colloid Interface Sci.* **36**, 18-23 (1971).
17. de Kruif, C.G., Weinbreck, F. & de Vries, R. Complex coacervation of proteins and anionic polysaccharides. *Curr. Opin. Colloid. Interface Sci.* **9**, 340-349 (2004).
18. Antonov, M., Mazzawi, M. & Dubin, P.L., (2010) Entering and exiting the protein–polyelectrolyte coacervate phase via non-monotonic salt dependence of critical conditions. *Biomacromolecules* **11**, 51-59.
19. Koga, S., Williams, D.S., Perriman, A.W. & Mann, S. Peptide-nucleotide microdroplets as a step towards a membrane-free protocell model. *Nat. Chem.* **3**, 720–724 (2011).
20. Tang, T-Y.D., Antognozzi, M., Vicary, J.A., Perriman, A.W. & Mann, S. Small-molecule uptake in membrane-free peptide/nucleotide protocells. *Soft Matter* **9**, 7647-7656 (2013).
21. Brangwynne, C.P., Mitchison, T.J. & Hyman, A.A. Active liquid-like behavior of nucleoli determines their size and shape in *Xenopus laevis* oocytes. *Proc. Natl. Acad. Sci. USA.*

- 108**, 4334–4339 (2011).
22. Hyman, A.A. & Simons, K. Cell biology. Beyond oil and water—phase transitions in cells. *Science* **337**,1047–1049, (2012).
 23. Sokolova, E., Spruijt, E., Hansen, M.M.K., Dubuc, E., Groen, J., Chokkalingam, V., Piruska, A., Heus, H.A. & Huck, W.T.S. Enhanced transcription rates in membrane-free protocells formed by coacervation of cell lysate. *Proc. Natl. Acad. Sci. USA*. doi/10.1073/pnas.1222321110 (2013).
 24. Strulson, C.A., Molden, R.C., Keating, C.D. & Bevilacqua, P.C. RNA catalysis through compartmentalization. *Nat. Chem.* **4**, 941–946 (2012).
 25. Crosby, J., Treadwell, T., Hammerton, M., Vasilakis, K., Crump, M.P., Williams, D.S. & Mann, S. Stabilization and enhanced reactivity of actinorhodin polyketide synthase minimal complex in polymer/nucleotide coacervate droplets. *Chem. Commun.* **48**, 11832-11834 (2012).
 26. Johnson, I.D., Kang, H.C. & Haugland, R.P. Fluorescent membrane probes incorporating dipyrrometheneboron difluoride fluorophores. *Anal. Biochem.* **198**, 228-37 (1991).
 27. Kasurinen, J. A novel fluorescent fatty acid, 5-methyl-BDY-3-dodecanoic acid, is a potential probe in lipid transport studies by incorporating selectively to lipid classes of BHK cells. *Biochem. Biophys. Res. Commun.* **187**, 1594-601 (1992).
 28. Rogers, R.A., Jack, R.M. & Furlong, S.T. Lipid and membrane protein transfer from human neutrophils to schistosomes is mediated by ligand binding. *J. Cell. Sci.* **106**, 485-91 (1993).
 29. Williams, D.S., Koga, S., Hak, C.R C., Majrekar, A., Patil, A.J., Perriman, A.W & Mann, S. Polymer/nucleotide droplets as bio-inspired functional micro- compartments. *Soft Matter*, **8**, 6004-6014 (2012).
 30. Hosny, N.A., Fitzgerald, C., Tong, C., Kalberer, M., Kuimova, M.K. & Pope, F.D., Fluorescent lifetime imaging of atmospheric aerosols : A direct probe of aerosol viscosity. *Faraday discussions* DOI: 10.1039/C3FD00041A (2013)
 31. Wu, Y., Stefl, M., Olyska, A., Hof, M., Yahioglu, G., Yip, P., Casey, D., Ces, O. & Humpolickova, J., Kuimova, M.K. Molecular rheometry: direct determination of viscosity in Lo and Ld lipid phases via fluorescence lifetime imaging. *Phys. Chem. Chem. Phys.* **15**, 14986-93 (2013)
 32. Hosny, N.A., Mohamedi, G., Rademeyer, P., Owen, J., Wu, Y., Tang M-X., Eckersley, R.J., Stride, E. & Kuimova, M.K., Mapping microbubble viscosity using fluorescence lifetime imaging of molecular rotors. *Proc. Natl. Acad. Sci. USA.* **110**, 9225-9230 (2013).
 33. Panizza, A., Roux, D., Vuillaume, V., Lu, C-Y.D. & Cates, M.E. Viscoelasticity of the Onion Phase *Langmuir* **12**, 249-252 (1996).
 34. Pommella, A., Caserta, S. & Guido, S. Dynamic flow behaviour of surfactant vesicles under shear flow : role of a multilamellar microstructure. *Soft matter* **9**, 7545-7552 (2013).

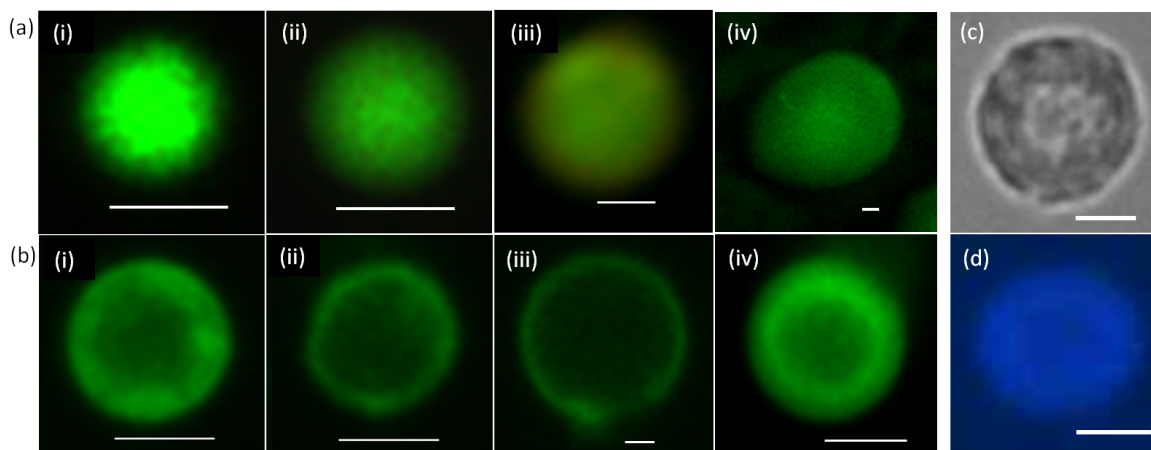


Figure 1: Fatty acid membrane self-assembly on the surface of positively charged coacervate micro-droplets. Fluorescence microscopy images of single droplets stained with the lipid soluble BODIPY FL C₁₆ dye. **(a)** Non-coated micro-droplets showing homogeneous fluorescence throughout the interior of the micro-compartments; (i) polylysine/RNA (monomer molar ratio 1 : 0.5), (ii) oligolysine/RNA (monomer molar ratio 1 : 0.25), (iii) oligolysine/ATP (monomer molar ratio 1 : 0.17), (iv) PDDA/ATP (monomer molar ratio 1 : 0.25). **(b)** Oleate-coated droplets prepared from (i) polylysine/RNA (pH 9, final mole ratio = 0.67 : 1 : 0.5), (ii) oligolysine/RNA (pH 9.3, 0.67 : 1 : 0.25), (iii) oligolysine/ATP (pH 8.7, 0.8 : 1 : 0.17) and (iv) PDDA/ATP (pH 10, 0.8 : 1 : 0.25) showing assembly of a fatty acid membrane specifically at the surface of the micro-compartments. All scale bars are 1 μ m. **(c,d)** oleate/PDDA/ATP micro-droplets prepared at a monomer molar ratio of 1.6 : 1 : 0.25 and doped with 0.1 mol% TNP-ATP; **(c)** bright field image of a single droplet, and **(d)** corresponding fluorescence microscopy image showing blue fluorescence from the TNP-ATP nucleotide in the fatty acid-encapsulated coacervate matrix; scale bars, 2 μ m.

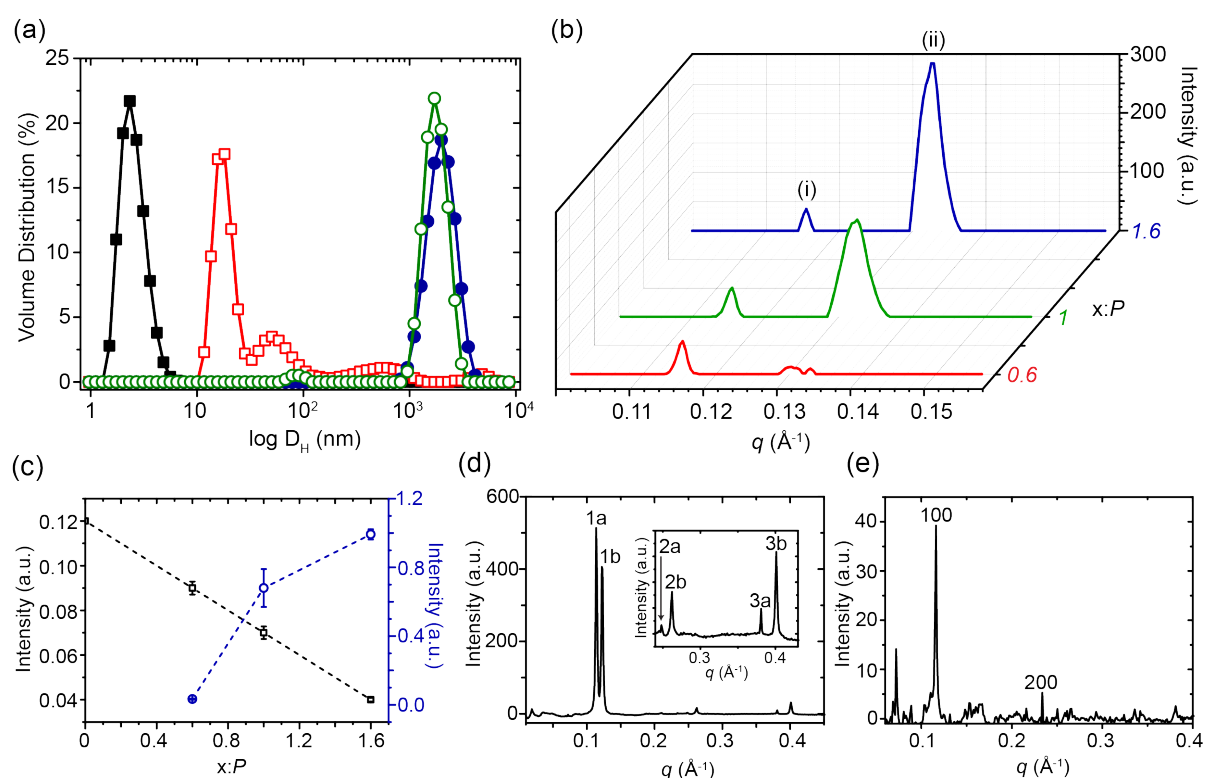


Figure 2: DLS and SAXS measurements on fatty acid membrane-coated coacervate droplets. (a) DLS profiles showing volume distributions of hydrodynamic diameters (D_H/nm) for oleate micelles (black filled squares, 20 mM oleate, pH 11), oleic acid/oleate multilamellar vesicles (red open squares, 20 mM, pH 8), uncoated PDDA/ATP micro-droplets (blue filled circles, PDDA : ATP molar ratio = 1 : 0.25 = P , pH 10) and oleate-coated PDDA/ATP micro-droplets (green open circles, 1.6 : P , pH 10.4). (b) SAXS profiles of oleate/PDDA/ATP micro-droplets prepared at 0.6 : P , 1.0 : P or 1.6 : P at pH 10 showing non-related Bragg reflections at 5.46 nm (peak (i)) and 4.77 nm (peak (ii)) and their dependence on increasing oleate concentration (increasing $x : P$). (c) Plot showing the changes in scattering peak intensity with increasing oleate concentration (increasing $x : P$) for the 5.46 nm (black open squares, left axis) and 4.77 nm (blue open circles, right axis) Bragg reflections shown in (b); error bars related to the deviation of the peaks from a Gaussian distribution. (d) SAXS profile of a concentrated dispersion of oleate/PDDA/ATP micro-droplets (1.6 : 1 : 0.25, pH 10.5) showing Bragg reflections corresponding to two multilamellar phases with interlayer spacings of $d_a = 5.51$ and $d_b = 5.06$ nm (peaks 1a, 2a, 3a and 1b, 2b, 3b, respectively). (e) SAXS profile for oleic acid/oleate vesicles prepared at pH 8 showing a multi-lamellar phase with an interlayer spacing of 5.5 nm.

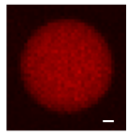
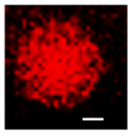
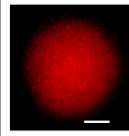
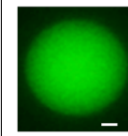
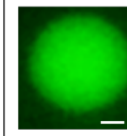
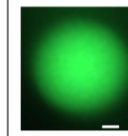
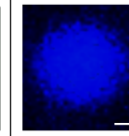
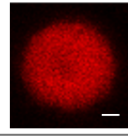
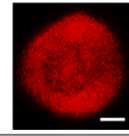
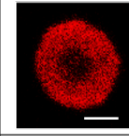
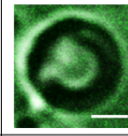
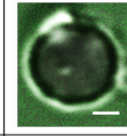
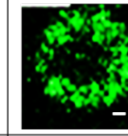
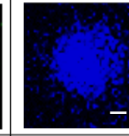
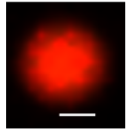
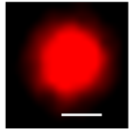
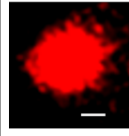
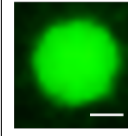
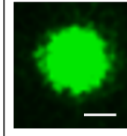
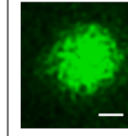
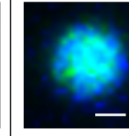
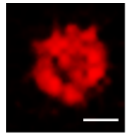
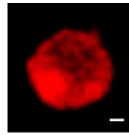
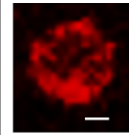
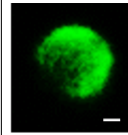
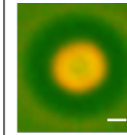
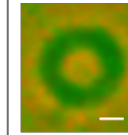
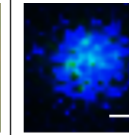
Dye	Methylene Blue	Rhodamine 6G	Kiton Red	Fluorescein	Calcein	eGFP	NADH	
Charge	cationic	cationic	zwitterionic	anionic	anionic	anionic	anionic	
Sample	Mw	320 g mol ⁻¹	479 g mol ⁻¹	581 g mol ⁻¹	332 g mol ⁻¹	623 g mol ⁻¹	32 700 g mol ⁻¹	663 g mol ⁻¹
PDDA / ATP 1 : 0.25 (molar ratio)								
Oleate / PDDA / ATP 1.6: 1 : 0.25 (molar ratio)								
Olys / RNA 1 : 0.25 (molar ratio)								
Oleate / Olys / RNA 0.7 : 1 : 0.25 (molar ratio)								

Figure 3: Molecular uptake/exclusion from fatty acid-coated PDDA/ATP and oligolysine/RNA coacervate micro-droplets. Table of confocal fluorescence microscopy images showing uncoated or oleate-coated coacervate single droplets exposed to various cationic, anionic or zwitterionic solutes present in the external continuous aqueous phase. Images displayed in rows corresponding to PDDA/ATP and oligolysine (Olys)/RNA coacervates show homogeneous fluorescence throughout the droplets indicating that the chromophores are sequestered into the interior of the membrane-free protocells. In contrast, the images shown in the rows for oleate/PDDA/ATP and oleate/oligolysine/RNA display fluorescence only at the surface of the membrane-coated droplets (cationic dyes) or minimal fluorescence (anionic solutes), indicating that the chromophores are excluded from the droplet interior. The exceptions are methylene blue and NADH, which are taken up into the membrane-coated droplets. All scale bars, 1 μm .

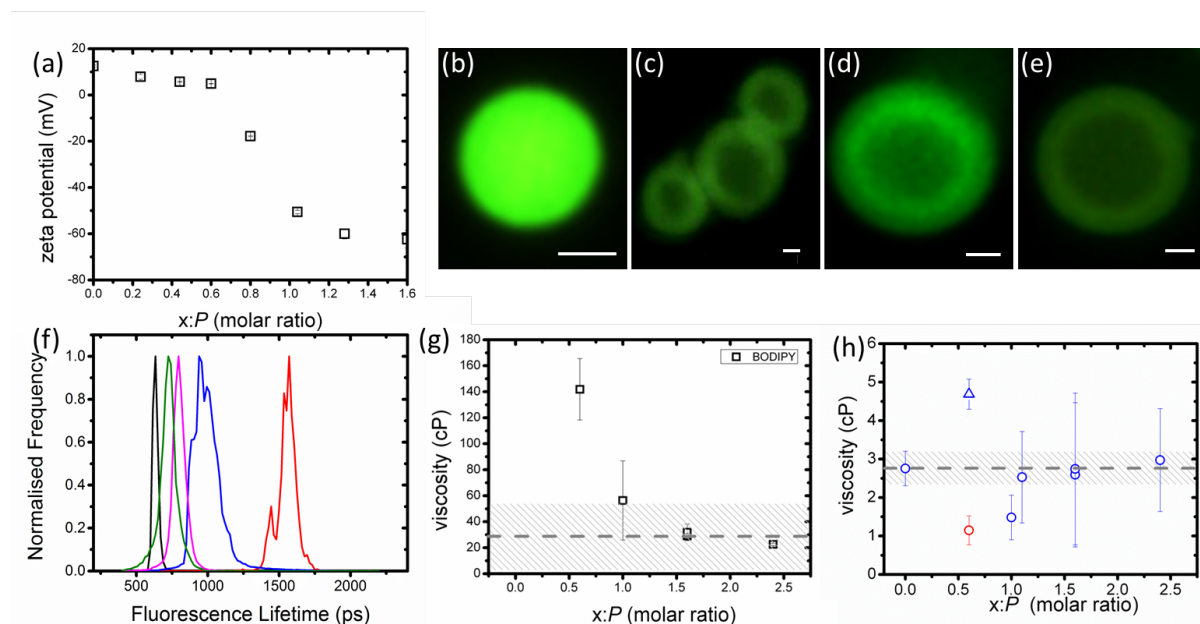


Figure 4: Mechanism of coacervate-mediated membrane assembly. (a) Plot of zeta potential for PDDA/ATP micro-droplets prepared at various oleate (x): PDDA : ATP monomer molar ratios ($x : P$, where $P = \text{PDDA} : \text{ATP} = 1 : 0.25$). Lowering of the surface charge due to electrostatic binding results in charge neutralization followed by charge reversal. (b-e) Fluorescence microscopy images of oleate-coated PDDA/ATP droplets stained with lipid-soluble BODIPY FL C₁₆ dye at $0.32 : P$ (b), $0.4 : P$ (c), $1.0 : P$ (d) and $1.6 : P$ (e); all scale bars, $1\mu\text{m}$. Note the presence of dye sequestration in (b) and membrane formation in (c-e). (f) Fluorescence lifetime distributions for membrane-solubilised BODIPY C₁₀ in oleate-coated PDDA/ATP micro-droplets prepared at pH 10 and the following molar ratios: $0.6 : P$ (red), $1 : P$ (blue), $1.6 : P$ (magenta), $2.4 : P$ (green). The control data for BODIPY C₁₀ in oleic acid/oleate vesicles at pH 8 is shown in black. Note the narrowing of the lifetime distribution and trend towards the lifetime observed in oleic acid/oleate vesicles as the $x : P$ ratio increases. (g) Plot of membrane viscosities (cP) derived from the fluorescence lifetime data shown in (f); grey bar indicates the viscosity of the oleic acid/oleate vesicles at pH 8 (see Fig. S11). Note that the error bars are mainly due to the viscosity distribution in each image rather than a low measurement accuracy. (h) Plot of viscosity derived from the lifetime of Kiton red associated with the PDDA/ATP interior of uncoated ($0 : P$) or oleate-coated micro-droplets at various oleate (x) : P molar ratios. Data points at $0.6 : P$ (blue triangle and red circle) are anomalous due to charge neutral conditions. Note that the identical point in (g) also shows an anomalous oleate viscosity. Both datasets suggest instability of the micro-droplets under these conditions. Error bars in (g) and (h) represent standard deviations.

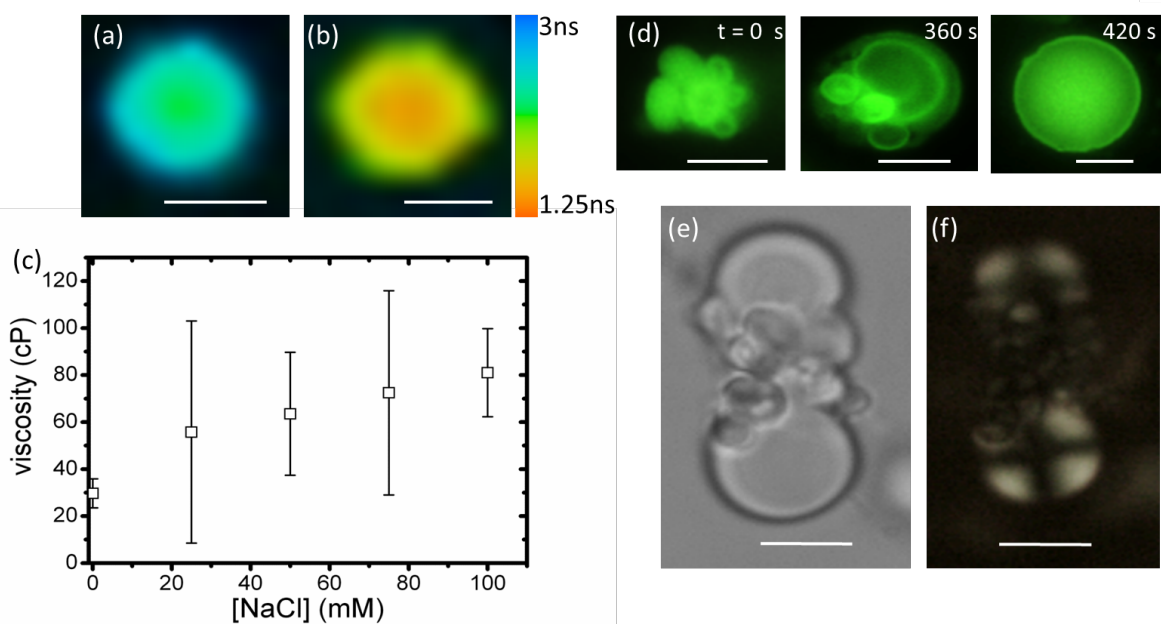


Figure 5: Ionic strength-induced coacervate disassembly and oleate membrane fusion in hybrid protocells. (a,b) Fluorescence lifetime maps for oleate/PDDA/ATP micro-droplets (monomer molar ratio = 1.6 : 1 : 0.25) containing Kiton red in the absence (a) or presence (b) of 75 mM NaCl. The images show a marked reduction in the fluorescence lifetimes due to a reduction in the viscosity of the compartmentalized medium associated with the salt-induced disassembly of the membrane-enclosed coacervate; scale bars, 5 μ m. (c) Plot of membrane viscosity derived from fluorescence lifetime maps as a function of NaCl concentration; error bars represent standard deviations. (d) Time sequence showing fluorescence images of BODIPY FL C₁₆-stained oleate/PDDA/ATP micro-droplets (monomer molar ratio = 1.6 : 1 : 0.25) after the addition of 100 mM NaCl at $t = 0$, 360 and 420 s. Aggregation of the oleate-coated micro-droplets occurs immediately after addition of salt and results in fusion and growth of the micro-compartments; the presence of the fluorescence dye throughout the fused micro-droplets is indicative of the formation of densely packed multilamellar “onion” vesicles; scale bars = 5 μ m. (e) Bright field and (f) cross-polarised microscopy images of oleate/PDDA/ATP micro-droplets in the presence of 100 mM NaCl showing maltese cross textures characteristic of multilamellar “onion” vesicles; scale bars, 5 μ m.